JOURNAL OF GEOPHYSICAL RESEARCH, VOL. 116, C11023, doi:10.1029/2011JC006970, 2011

Prediction of the diurnal warming of sea surface temperature using an atmosphere-ocean mixed layer coupled model

Yign Noh,[1] Eunjeong Lee,[1] Dong-Hoon Kim,[1] Song-You Hong,[1] Mee-Ja Kim,[2] and Mi-Lim Ou[2]

Received 21 January 2011; revised 3 September 2011; accepted 12 September 2011; published 16 November 2011.

[1] An atmosphere-ocean mixed layer coupled model is developed to predict the diurnal variability of sea surface temperature (SST). For this purpose, a new mixed layer model is developed, which is able to reproduce realistic temperature profiles under the various atmospheric conditions, ranging from the formation of a diurnal thermocline under strong wind to the appearance of strong near surface stratification under weak wind. The predicted diurnal warming of SST (ΔSST) from the model is compared with satellite and buoy data in various aspects, including scatterplots, time series, and probability density functions of ΔSST, in order to examine the predictability. The model performance is also compared with other model results. In addition the diurnal variation of temperature profiles below the sea surface, whose information is not available from satellite data, is investigated based on model output.

Citation: Noh, Y., E. Lee, D.-H. Kim, S.-Y. Hong, M.-J. Kim, and M.-L. Ou (2011), Prediction of the diurnal warming of sea surface temperature using an atmosphere-ocean mixed layer coupled model, *J. Geophys. Res.*, *116*, C11023, doi:10.1029/2011JC006970.

1. Introduction

[2] The diurnal variation of sea surface temperature (SST), caused by insolation, is a key process controlling air-sea interaction. The diurnal warming of SST, ΔSST, is usually less than 1 K, but often reaches a few degrees under the conditions of weak wind and strong insolation, as the downward heat transport from the sea surface is suppressed in the absence of turbulent mixing. Sometimes it exceeds 5 K under extreme conditions [*Flament et al.*, 1994; *Merchant et al.*, 2008].

[3] Currently, most numerical weather predictions (NWP) are calculated based on the daily mean SST without considering the diurnal variation of SST. It has been reported, however, that its diurnal warming can increase the surface heat flux by the order of 10 W m^{-2} [*Fairall et al.*, 1996], and thus influences the atmospheric variability from diurnal to intraseasonal time scale [see, e.g., *Kawai and Wada*, 2007; *Webster et al.*, 1996]. Accordingly, several researchers have suggested that the inclusion of the diurnal variation of SST is important in NWP to reproduce the proper atmosphere-ocean coupled dynamics [*Dai and Trenberth*, 2004; *Shinoda*, 2005; *Bernie et al.*, 2005; *Woolnough et al.*, 2007; *Bellenger et al.*, 2010]. Furthermore, the information on the diurnal variability of SST is essential to merge satellite-derived SSTs, which are measured at different local times of the day [*Donlon et al.*, 2007].

[4] The observation of the diurnal warming of SST has been carried out by in situ or satellite measurements [*Stommel et al.*, 1969; *Cornillon and Stramma*, 1985; *Price et al.*, 1986; *Webster et al.*, 1996; *Stuart-Menteth and Robinson*, 2003; *Clayson and Weitlich*, 2007; *Gentemann et al.*, 2008]. Although satellite measurements have an advantage of providing information on the SST over the global scale, unlike in situ measurements, they still have many limitations. For example, information is not available either under the cloudy condition (e.g., satellites with infrared sensors), or for the diurnal variation (e.g., polar orbiting satellites). Furthermore, they cannot provide information of subsurface temperature profiles.

[5] The prediction of ΔSST has been attempted by using mixed layer models which predict temperature profiles by calculating vertical heat transport [*Kawai and Kawamura*, 2000; *Clayson and Chen*, 2002; *Zeng and Beljaars*, 2005; *Pimentel et al.*, 2008; *Takaya et al.*, 2010], bulk models which consider the total heat content of the warming layer [*Price et al.*, 1986; *Fairall et al.*, 1996; *Gentemann et al.*, 2009], and regression models based on the daily mean or peak values of atmospheric forcing [*Webster et al.*, 1996; *Kawai and Kawamura*, 2002, 2003; *Gentemann et al.*, 2003; *Clayson and Weitlich*, 2007].

[6] Traditionally, the prediction of ΔSST has been examined for a particular location, while comparing with in situ measurement data. However, satellite data allows us to examine the prediction of ΔSST over large regions now [*Stuart-Menteth and Robinson*, 2003; *Tanahashi et al.*, 2003; *Gentemann et al.*, 2003; *Zeng and Beljaars*, 2005;

[1]Department of Atmospheric Sciences/Global Environmental Laboratory, Yonsei University, Seoul, South Korea.
[2]National Institute of Meteorological Research, Seoul, South Korea.

0148-0227/11/2011JC006970

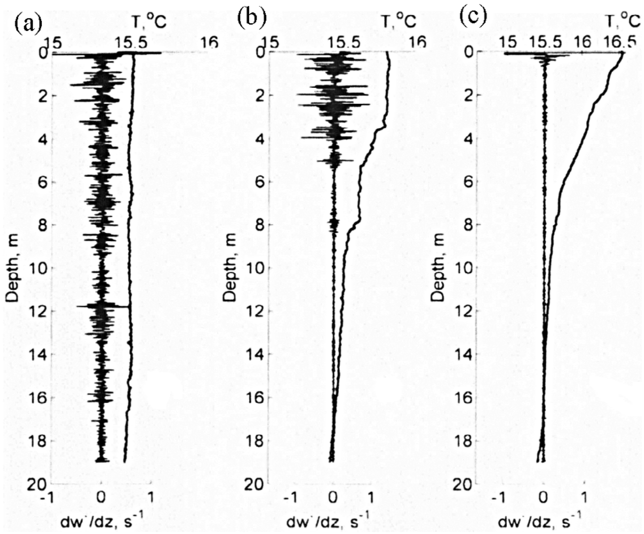

Figure 1. Examples of temperature T and strain fluctuation dw'/dz profiles under different wind conditions observed in the North Atlantic near 46°N, 20°W in June, 1998. (a) U_{18} = 8.3 m s^{-1}, H_0 = 42 W m^{-2}; (b) U_{18} = 6.2 m s^{-1}, H_0 = 103 W m^{-2}; (c) U_{18} = 3.3 m s^{-1}, H_0 = 100 W m^{-2}. U_{18} is the wind speed at 18 m height, and different temperature scales are used in each figure. From *Soloviev and Lukas* [2006] with kind permission from Springer Science+ Business Media B.V.

Kawai and Kawamura, 2005; *Pimentel et al.*, 2008; *Takaya et al.*, 2010]. For the prediction of ΔSST, the atmospheric forcing for the model was provided either by satellite data or by NWP model results calculated beforehand based on the daily mean SST. In these cases the atmospheric forcing data are available only at a certain time interval; for example, 6 h by *Pimentel et al.* [2008]. No attempt has been made as yet to predict ΔSST over large regions using an atmosphere-ocean mixed layer coupled model.

[7] Atmosphere-ocean mixed layer coupled models realize the interaction between the atmosphere and the upper ocean effectively, when the heat transport by ocean circulation is negligible as in the case of the diurnal variation of SST. A coupled model can provide continuous information of SST and temperature profiles, regardless of the cloud condition, and thus contributing to complement satellite data. Coupled models can also contribute to improve the performance of the NWP model by realizing more realistic air-sea interaction.

[8] There have been several previous attempts to develop atmosphere-ocean mixed layer coupled models [*Price et al.*, 1994; *Haarsma et al.*, 2005; *Woolnough et al.*, 2007; *Davis et al.*, 2008; *Duan et al.*, 2008; *Lebeaupin Brossier and Drobinski*, 2009]. The purpose of coupling has been mainly to improve the prediction of hurricanes or the Madden-Julian Oscillation, however, rather than to predict the diurnal variability of SST.

[9] In the ocean mixed layer, strong turbulence usually exists near the sea surface as a result of wave breaking. As a result, in response to surface heating, a diurnal thermocline is formed at a certain depth while a well mixed layer is maintained near the surface [*Delnore*, 1972; *Stommel et al.*, 1969; *Brainerd and Gregg*, 1993; *Noh*, 1996; *Noh et al.*, 2009]. However, under conditions of very weak wind, wave breaking cannot occur any more, and the downward heat transport from the surface is suppressed in the absence of turbulence. As a result, a strong temperature gradient appears near the surface responding to surface heating. In this case there appears a significant difference between the temperature at the sea surface, measured by a satellite, and the temperature at 1 m depth, measured by ships and buoys. For example, Figures 1b and 1c, obtained by *Soloviev and Lukas* [2006], show temperature profiles corresponding to former and latter cases, respectively. Similar contrasting profiles are also found by *Soloviev and Lukas* [1997], *Donlon et al.* [2002], and *Gentemann et al.* [2009].

[10] The latter case is particularly important in the prediction of ΔSST, because it corresponds to the case where the largest ΔSST appears. Therefore, in order to predict ΔSST properly, it is essential for the mixed layer model to reproduce realistic temperature profiles under surface heating in the case of weak wind as well as of strong wind.

[11] Section 2 describes the atmosphere-ocean mixed layer coupled model. Here a new ocean mixed layer model is developed to predict the diurnal variation of SST properly. Section 3 describes satellite data. The performance of a new mixed layer model is examined under idealized surface heating in section 4.1. The predicted ΔSST from the coupled model is described in section 4.2, and verified in comparison with satellite and buoy data and other model results in section 4.3. Finally, the distribution of temperature below the surface is presented from model output in section 4.4.

2. Model and Simulation

2.1. Atmospheric Model

[12] The Weather Research and Forecasting (WRF) model version 3.1 is used for the atmosphere model [*Skamarock et al.*, 2008]. The model has 25 km horizontal resolution and 31 vertical levels. The domain covers East Asia (110–150°E, 11–61°N). Initial and lateral conditions are given by the National Center for Environmental Prediction (NCEP) reanalysis data [*Kalnay et al.*, 1996]. Exchange of fluxes at the sea surface between the atmosphere and ocean mixed layer model is carried out every 120 s.

[13] The microphysical scheme uses the WRF Single-Moment 3-class scheme [*Hong et al.*, 2004]. Convection is parameterized by the new Kain-Fritsch convective scheme [*Kain*, 2004], and the turbulence scheme is the Yonsei University (YSU) planetary boundary layer scheme [*Noh et al.*, 2003]. The radiative scheme is the Rapid Radiative Transfer Model (RRTM) [*Mlawer et al.*, 1997] for the long wave flux and the Dudhia parameterization [*Dudhia*, 1989] for the short wave flux.

2.2. Ocean Mixed Layer Model

[14] The new ocean mixed layer model is based on the Noh model, which reproduces well the realistic upper ocean structure [e.g., *Noh and Kim*, 1999; *Noh et al.*, 2002, 2005; *Hasumi and Emori*, 2004; *Duan et al.*, 2008; *Rascle and

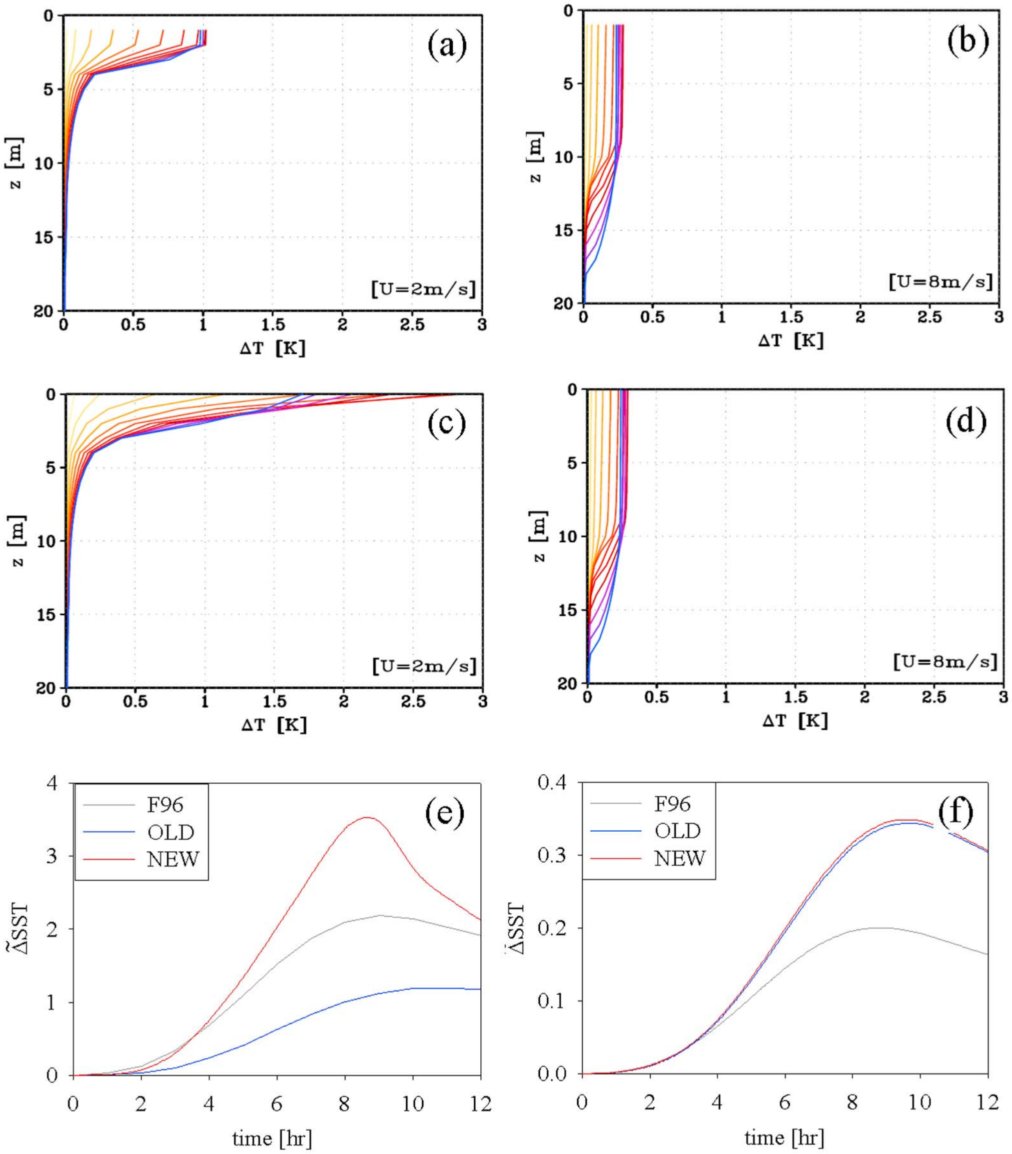

Figure 2. Evolutions of temperature profiles after the onset of surface heating: (a, b) the old model and (c, d) the new model. (Δt = 1 h) and variations of $\tilde{\Delta}$SST (SST(t) − SST(0)) with time. (e, f) Red lines represent the new model, blue lines represent the old model, and black lines represent the model by *Fairall et al.* [1996] (F96). Surface heat flux H is given by $H = H_0[1 - \cos(2\pi t/T)]$ with $H_0 = 350$ W m^{-2} and $T = 12$ h. In Figures 2a, 2c, and 2e, $U = 2$ m s^{-1}. In Figures 2b, 2d, and 2f, $U = 8$ m s^{-1}.

Ardhuin, 2009] and shows a good agreement with large eddy simulation (LES) results [*Noh et al.*, 2004, 2009, 2010, 2011]. The model is a turbulence closure model using eddy diffusivity and viscosity, similar to the Mellor-Yamada model [*Mellor and Yamada*, 1982], but reproduces a uniform mixed layer, consistent with bulk models [e.g., *Niiler and Kraus*, 1977], by taking into account the effects of wave breaking and Langmuir circulation.

[15] In the model the eddy viscosity and diffusivity are calculated by

$$K_m = S_m q l \tag{1}$$

$$K_h = S_h q l, \tag{2}$$

using the velocity scale q and length scale l of turbulence, respectively. Here S_m and S_h are empirical constants, and l is prescribed by

$$\frac{1}{l} = \frac{1}{\kappa(z + z_0)} + \frac{1}{h}, \tag{3}$$

where z_0 is the roughness length scale at the sea surface ($z = 0$ m), κ is the von Karman constant, and h is the mixed layer depth. In order to calculate q, turbulent kinetic energy (TKE) equation is solved.

[16] At the surface the TKE flux F and the length scale z_0 are given by $F = mu_*^3$ with $m = 100$, and $z_0 = 1$ m, following *Craig and Banner*'s [1994] analysis of the observed near

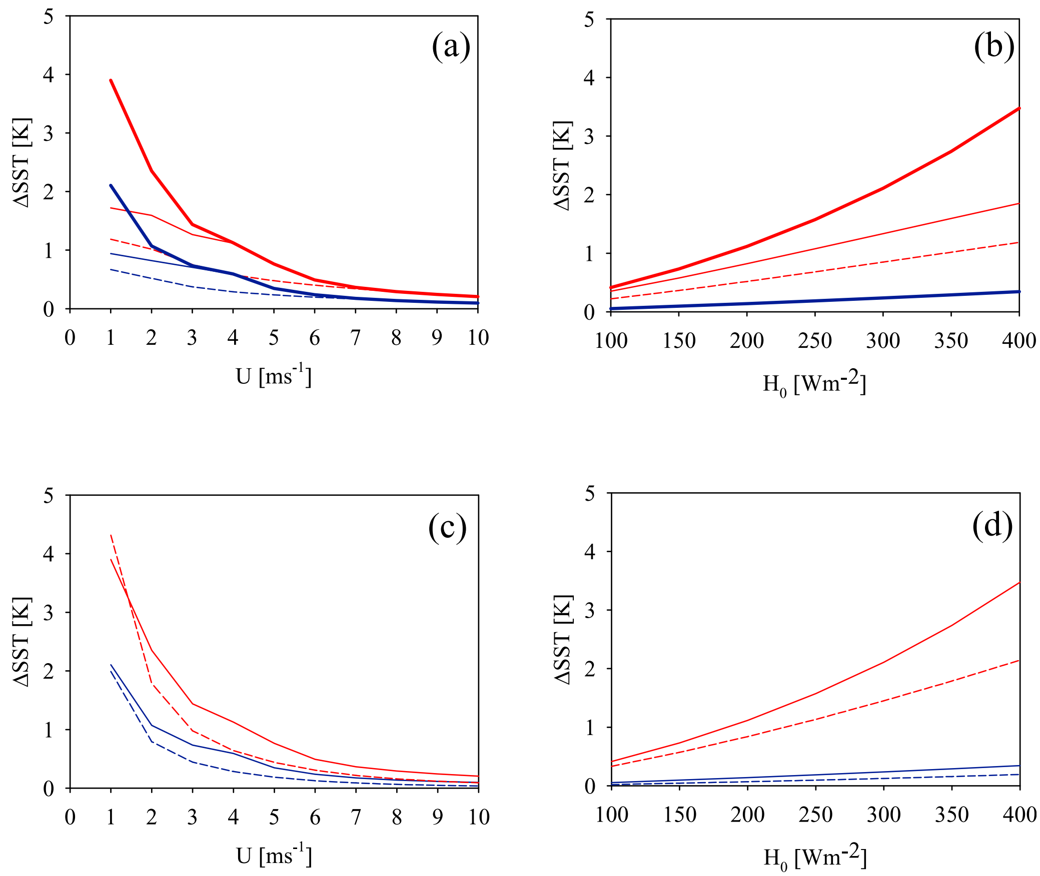

Figure 3. (left) Variations of ΔSST with U. Red lines show H_0 = 350 W m^{-2} and blue lines show H_0 = 200 W m^{-2}. (right) Variations of ΔSST with H_0. Red lines show U = 2 m s^{-1} and blue lines show U = 8 m s^{-1}. (a, b) Bulk SST from the old model (dashed line), bulk ΔSST from the new model (thin line), skin ΔSST from the new model (thick line). (c, d) Skin ΔSST from the new model (solid line) and F96 (dashed line).

surface turbulence structure affected by wave breaking. Here u_* is the frictional velocity.

[17] Since TKE production is dominated by the TKE flux within the mixed layer in the presence of Langmuir circulation [*Noh et al.*, 2011], rather than shear production, the effect of stratification is parameterized in terms of the Richardson number based on TKE itself, i.e., Rt (= $(Nl/q)^2$), instead of the conventional Ri (= $(N/S)^2$); i.e.,

$$S_m/S_{m0} = (1 + \alpha \mathrm{Rt})^{-1/2}. \quad (4)$$

Here N is the Brunt-Väisälä frequency, S is the mean velocity shear, and S_{m0} is the value of S_m in (1) in the absence of stratification. The relation (4) is confirmed by LES with the empirical constant $\alpha \cong 50$ [*Noh et al.*, 2011]. Similar parameterizations to (4) are also applied to S_h in (2). For the detailed description of the model, one can refer to *Noh and Kim* [1999].

[18] However, this model considers only the case where the wind stress is sufficiently strong to generate wave breaking. When the wind stress becomes very weak, wave breaking cannot occur any more, and the turbulence structure near the sea surface becomes similar to that near the solid-wall boundary in which F disappears and z_0 is much smaller. Incorporation of this case is necessary to predict ΔSST, because it corresponds to the case where the largest ΔSST occurs.

[19] In order to allow the transition to the case without wave breaking, we modify the formulae for F and z_0 as

$$F = mu_*^3\left[1 - \exp\{-(\beta u_*/C)^n\}\right], \quad (5)$$

$$z_0 = \hat{z}_0\left[1 - \exp\{-(\beta u_*/C)^n\}\right], \quad (6)$$

where C is the characteristic phase velocity of surface waves, β is a proportional constant and $\hat{z}_0$ is the roughness length scale under strong wave breaking ($\hat{z}_0$ = 1 m). Since wave breaking occurs typically when u/C exceeds a certain value, where u is the fluid velocity at the surface [*Melville*, 1996], we assume that the suppression of wave breaking affects F and z_0 through u_*/C. We have found that, with $n = 6$ and $\beta/C = 150$, the rapid transition to the case without wave breaking occurs at $u_* \sim 0.003$ m s^{-1}, which is consistent with

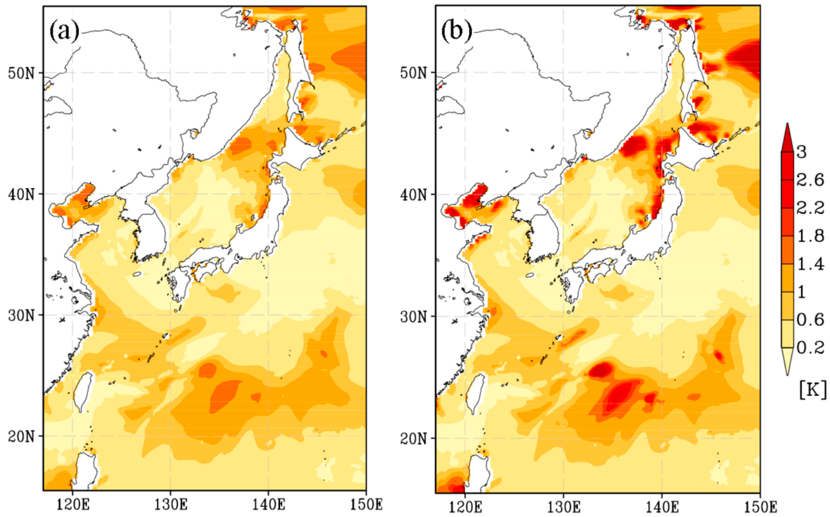

Figure 4. Distributions of ΔSST from the coupled model (June 5, 2008). (a) Bulk ΔSST and (b) skin ΔSST.

the fact that whitecaps generated by wave breaking are observed to begin at a wind speed of approximately 3 m s^{-1} [*Melville*, 1996].

[20] Another problem in this case is that the vertical resolution as small as 0.03 m is necessary to reproduce the large temperature gradient near the surface under the condition of weak wind and strong insolation and to predict skin SST correctly [e.g., *Pimentel et al.*, 2008]. Such a high resolution is not desirable in the atmosphere-ocean mixed layer coupled model, and Δz = 1 m is used in the present model with total 100 vertical levels.

[21] Instead we assume the shape of a temperature profile in the warm layer, following *Zeng and Beljaars* [2005, hereinafter ZB05], as

$$T(z) = T_s - (z/d)^{\nu}[T_s - T_d], \tag{7}$$

where T_s is the temperature at the surface (z = 0 m) and T_d is the temperature at $z = d$. We choose the empirical constants as d = 2 m, which corresponds to the thickness of the first two grids. The mean temperatures of the first and second grid, T_1 and T_2, are then given by

$$T_1 = T_s - \frac{2}{\nu+1}\left(\frac{1}{2}\right)^{\nu+1}(T_s - T_d) \tag{8}$$

$$T_2 = T_s - \frac{2}{\nu+1}\left[1 - \left(\frac{1}{2}\right)^{\nu+1}\right](T_s - T_d) \tag{9}$$

From (8) and (9), we can calculate T_s by

$$T_s = T_1 + \frac{1}{2^{\nu+1} - 2}(T_1 - T_2), \tag{10}$$

once T_1 and T_2 are calculated from the model. In the present work we will regard T_s and T_1 as the skin and bulk SST, respectively. According to the detailed definitions of SST proposed by *Donlon et al.* [2002], the bulk SST measured at 1-m depth is called as the 1-m depth SST. On the other

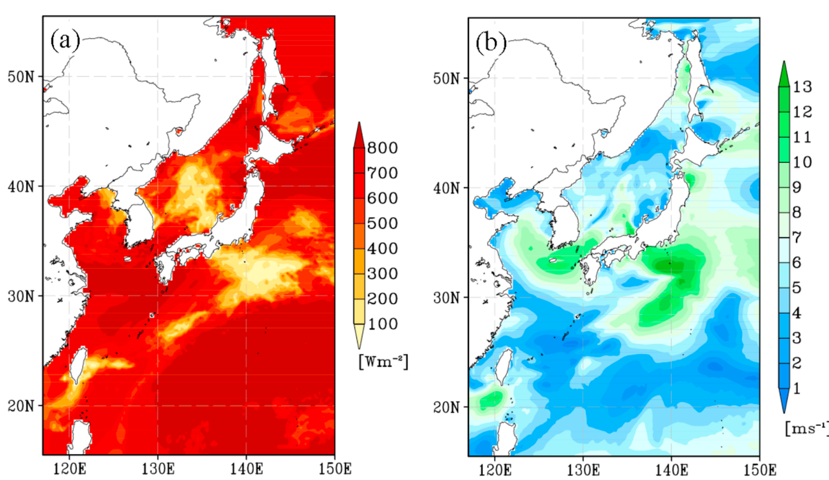

Figure 5. Distributions of atmospheric forcing from the coupled model (June 5, 2008). (a) Peak solar radiation and (b) daily mean wind speed at z = 10 m (U).

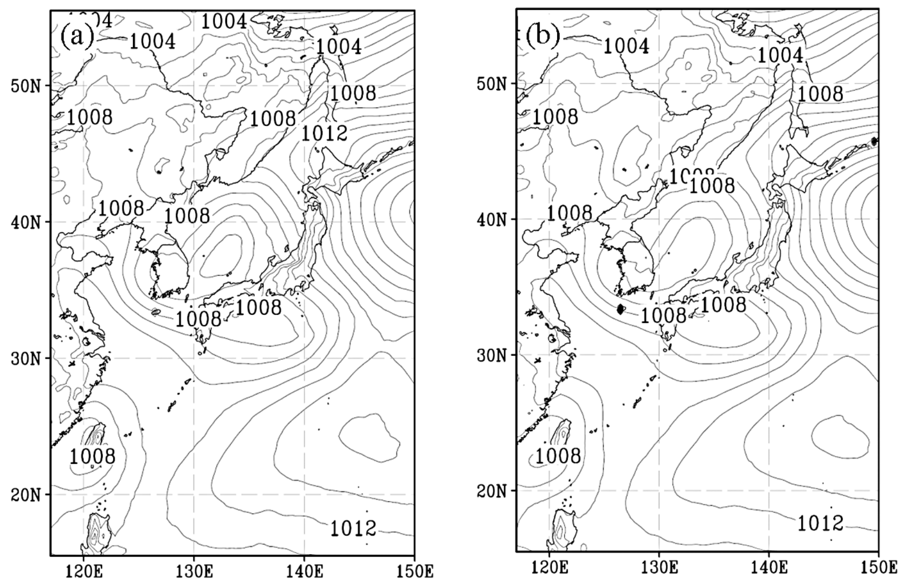

Figure 6. Comparison of daily mean sea level pressures (June 5, 2008). (a) Model and (b) observation.

hand, the bulk SST in the present work represents the mean temperature over the top 1 m.

[22] The temperature gradient between the first and second grid at $z = d/2$ is calculated by

$$\left.\frac{\partial T}{\partial z}\right|_{d/2} = -\nu\left(\frac{1}{2}\right)^{\nu-1}(T_s - T_d) = -\frac{\nu(\nu+1)}{2(2^\nu - 1)}\frac{T_1 - T_2}{d/2}, \quad (11)$$

which is used to calculate the heat flux between the first and second grid.

[23] Note that (10) and (11) become $T_s = T_1 + 0.5(T_1 - T_2)$ and $\partial T/\partial z = -(T_1 - T_2)/(d/2)$, if the temperature profile is linear ($\nu = 1$). *Zeng and Beljaars* [2005] suggested $\nu = 0.3$ regardless of the atmospheric condition. However, it is more reasonable to expect that ν approaches 1 for stronger wind stress and weaker surface heat flux. Accordingly we assume the formula for ν as

$$\nu = \exp(-\mu d/L), \quad (12)$$

with the optimized constant as $\mu = 0.02$, where L is the Monin-Obukhov length scale ($= u_*^3/Q$) and Q is the surface buoyancy flux. The minimum value of ν is set to be 0.3. In this way we can eliminate the excessive sensitivity of ΔSST

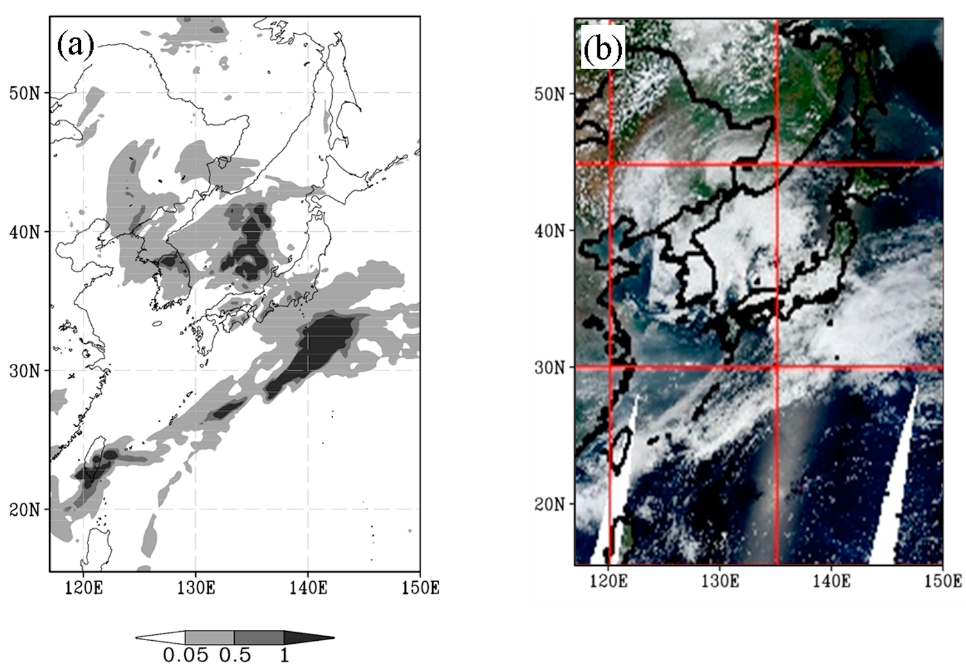

Figure 7. (a) Vertically integrated cloud and rainwater path (g m^{-2}) from the model and (b) corresponding satellite image (1100 LST, June 5, 2008).

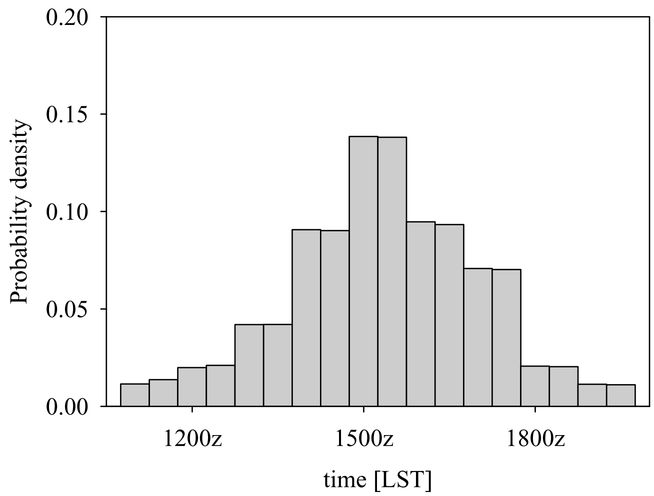

Figure 8. Probability density function of the time with the peak SST.

to wind stress by ZB05, which is pointed out by *Bellenger and Duvel* [2009] and *Takaya et al.* [2010]. Furthermore, (12) helps the new model recover the old model naturally with increasing L. The effect of cool skin layer is neglected, because only the case of diurnal heating is considered in the present work [*Ward and Donelan*, 2006]. The skin SST T_s calculated by (10), is also used to calculate latent and sensible heat fluxes in the coupled model.

[24] For the penetration of solar radiation, the nine-band model proposed by *Paulson and Simpson* [1981] and *Soloviev and Schlüssel* [1996] with Jerlov's water type II are used. The contribution from horizontal advection is neglected in the present model, because the present work focuses only on the diurnal variation on a relatively calm day; i.e., no hurricane.

[25] The initial condition of SST is given by the NCEP Final Analysis (FNL) data at 1800 GMT (0300 LST). The initial temperature profile is assumed to be uniform throughout the whole depth of the model (100 m). Salinity is assumed to be uniform throughout the whole depth with the climatological sea surface salinity from the FNL data, too. Note that the evolution of temperature profiles within the mixed layer responding to surface heating is not affected by the stratification below the mixed layer depth in the morning. The start of the model at 1800 GMT (0300 LST) helps to spin up the ocean until sunrise, while temperature profile remains uniform. Integration is carried out for each day during the period June 4–14, 2008. This period is chosen because of relatively calm weather and strong insolation before the start of monsoon season in this region.

3. Satellite and Buoy Data

[26] The SST data from Multifunctional Transport Satellite (MTSAT) - 1R are used for the comparison with model results in this study. MTSAT-1R is a Japanese geostationary satellite, which has been in operation since 2005 and flying 140°E and altitude of 35,800 km above the equator (http://mscweb.kishou.go.jp/general/activities/gms/index/htm). It provides visible/infrared imaginary for full disk coverage (60°N–60°S, 80°E–60°W), which covers East Asia and the western Pacific, with an hourly rate, and for the half hemisphere, every 30 min. The spatial resolution of satellite data is 4 km in the infrared channels at nadir. The satellite data is processed using the multichannel sea surface temperature (MCSST) method [*McClain et al.*, 1985] to estimate SST. For cloud detection, the algorithm using dynamic thresholds by *Dybbroe et al.* [2005] is applied.

[27] The drifting buoy SST data available from the Global Telecommunications Service (GTS) by the Data Buoy Cooperation Panel (DBCP) of the World Meteorological Organization (WMO) are used for the comparison with model results (http://www.jcommops.org/dbcp/data/access.html). The SST data were measured at about 1 m with the irregular sampling period. The match-up of MTSAT-1R SST data with buoy data results in root-mean square error (RMSE) 0.75 K and bias 0.14 K in the East Asian Region [*National Institute of Meteorological Research*, 2009].

4. Results

4.1. Response of the Mixed Layer Model to Idealized Surface Heating

[28] In section 2, the modification of the mixed layer model is described, which is aimed to reproduce strong stratification near the surface under weak wind and strong insolation. Figures 2a–2d compare the evolutions of temperature profiles under diurnally varying surface heating $H = H_0[1 - \cos(2\pi t/T)]$ with $H_0 = 350$ W m^{-2} and $T = 12$ h from the old and new mixed layer models, for the strong and weak wind speed ($U = 2$ and 8 m s^{-1}). In the present paper U represents the wind speed at $z = 10$ m, and is related to u_* via the empirical formula by *Smith* [1988]. In the new model temperature profiles are extended to z = 0 m, including T_s.

[29] When the wind is strong (U = 8 m s^{-1}), a diurnal thermocline is formed at a certain depth with time, while a well mixed layer is maintained near the surface, in both old and new models, similarly to the case of Figure 1b. It is also in agreement with observation data [*Brainerd and Gregg*, 1993; *Noh and Kim*, 1999] and LES results [*Noh et al.*, 2009]. On the other hand, when the wind is weak (U = 2 m s^{-1}), the strong temperature gradient, and consequently higher ΔSST, appears near the surface in the new model, similarly to Figure 1c, whereas a well mixed layer is still maintained in the old model. Meanwhile, it is interesting to observe the increase of the mixed layer depth and the decrease of SST in the afternoon, following the weakened surface heat flux, in Figure 2, consistent with observations by *Price et al.* [1986], *Soloviev and Lukas* [2006], and *Gentemann et al.* [2009]. Note that temperature profiles at t = 12 h in Figures 2a and 2b (blue lines) show the deeper mixed layer depth than those at the time of peak solar radiation (red lines). The afternoon deepening is more significant for stronger wind.

[30] The increases of SST since the onset of surface heating $\tilde{\Delta}$SST (= SST(t) − SST(0)) for the corresponding cases are shown in Figures 2e and 2f. Predictions from the bulk model by *Fairall et al.* [1996, hereinafter F96] are also included. Here SST is defined by T_s in the new model and by T_1 in the old model. Note that the mixed layer deepening in the afternoon causes SST to decrease in the later stage. In the new model the maximum SST appears earlier for $U = 2$ m s^{-1} by about an hour, reflecting that the response to

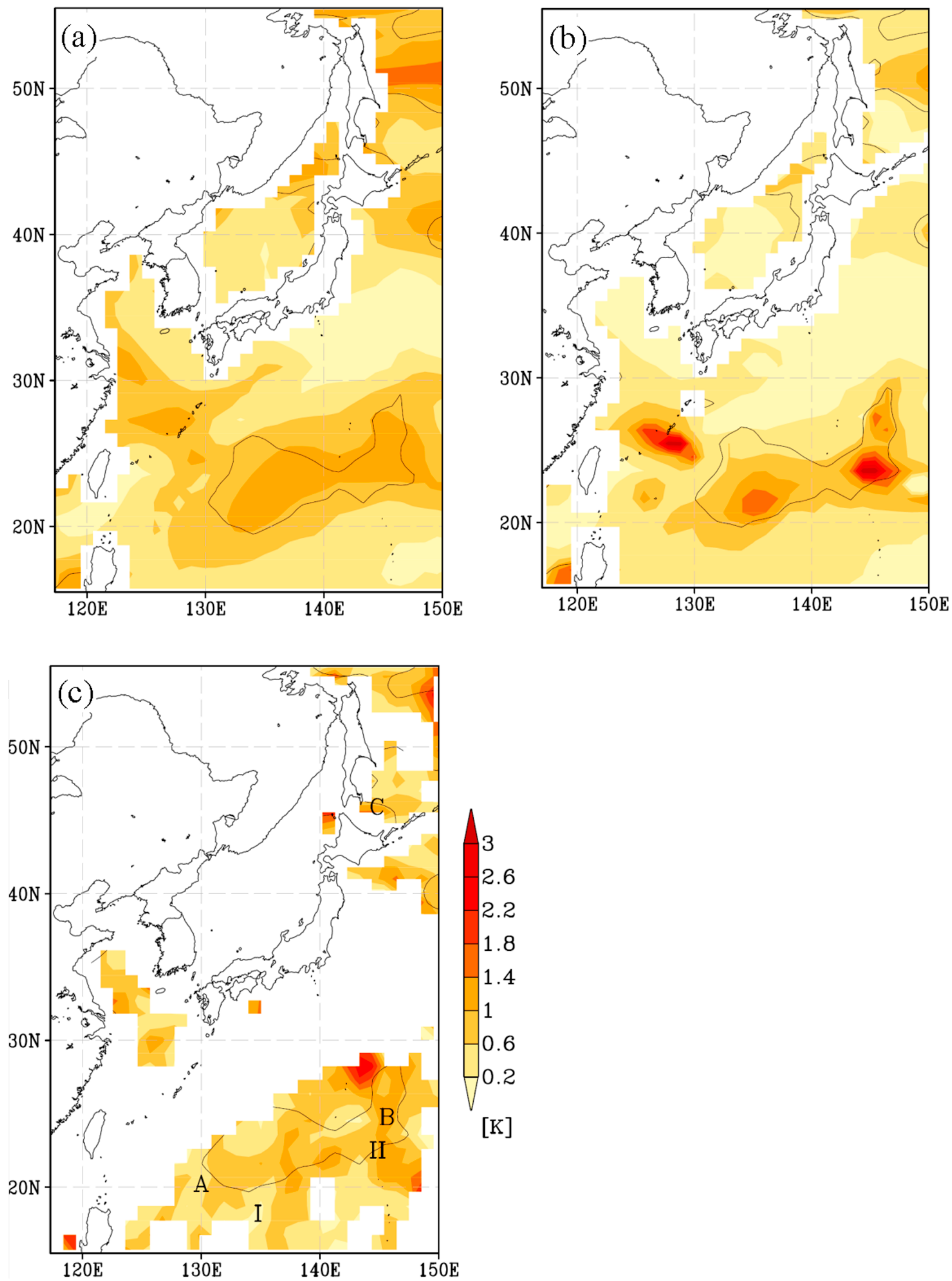

Figure 9. Distributions of ΔSST (contours of 1.0 K from the coupled model, shown in Figure 4, are overlapped for comparison; letters in Figure 9c represent the locations used for analysis in Figures 13 and 14). (a) Bulk ΔSST from KK03, (b) skin ΔSST from F96, and (c) skin ΔSST from satellite data (June 5, 2008).

the variation of surface heat flux is faster, when the affected thickness is shallower. On the other hand, the time with the maximum SST remains invariant which is discussed by F96. The maximum $\tilde{\Delta}$SST, i.e., ΔSST, from F96 is lower than ΔSST from the new model, although it is higher than ΔSST from the old model at $U = 2$ m s^{-1}. The underestimation of ΔSST by F96 is also reported in the previous work [*Gentemann et al.*, 2009]. Furthermore, Figures 2e and 2f reveal that the increase of SST found by F96 slows down in the later stage ($t > 6$ h), although it is comparable to the present model results in the initial stage ($t < 4$ h).

[31] By using the accumulated heat and momentum fluxes at the surface since the onset of surface heating, $[H]$ and $[u_*^2]$, F96 evaluates $\tilde{\Delta}$SST as

$$\tilde{\Delta}\mathrm{SST} = \frac{2[H]}{\rho c_p d_w}, \tag{13}$$

based on the assumption of linear temperature and velocity profiles up to the depth of a warm layer d_w. For the evaluation of d_w, the bulk Richardson number Ri (= $d_w g \alpha \Delta T/(\Delta u)^2$) is assumed to be constant following *Price et al.*

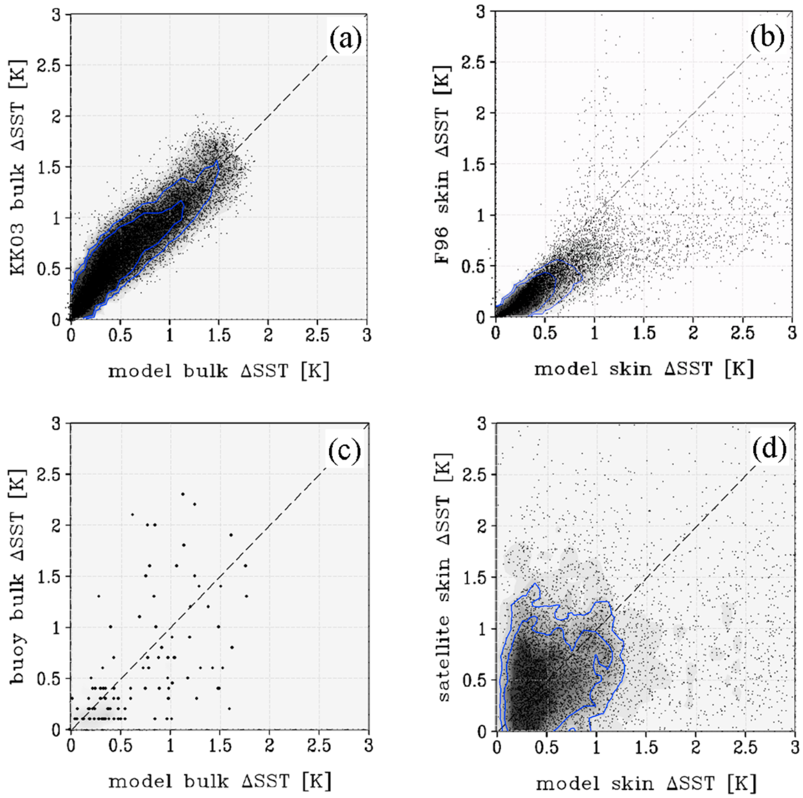

Figure 10. Scatterplots between ΔSSTs (for the scatterplot the values of ΔSST averaged over 1° × 1° grid cells are used). (a) Bulk ΔSST from the model versus KK03, (b) skin ΔSST from the model versus F96, (c) bulk ΔSST from the model versus buoy data, and (d) skin ΔSST from the model versus satellite data.

[1986], where ΔT and Δu are the differences of temperature and velocity between the surface and $z = d_w$, α is the thermal expansion coefficient, and g is the gravitational acceleration. It leads to

$$d_w = \left(\frac{2\mathrm{Ri}_c \rho c_p}{g\alpha}\right)^{1/2} \frac{\left[u_*^2\right]}{[H]^{1/2}}, \tag{14}$$

and $\mathrm{Ri}_c = 0.65$ is used for the critical value of Ri.

[32] Equation (14) implies that d_w grows with $t^{1/2}$, if H and u_* are constant, which is equivalent to constant eddy diffusivity. Generation of stratification under surface heating suppresses eddy diffusivity, and consequently the downward heat transport, however. As a result, the depth of a warm layer may not increase significantly with time, which is also expected from Figures 2a–2d. Note in particular that the depth of a diurnal thermocline is usually expected to remain invariant with time, for constant H and u_*, at a depth determined by the Monin-Obukhov length scale L [*Niiler and Kraus*, 1977; *Noh*, 1996]. The overestimated increasing rate of d_w by F96 may cause smaller $\widetilde{\Delta}$SST in the later stage, as shown in Figures 2e and 2f. The underestimation of $\widetilde{\Delta}$SST can be also caused by the stronger temperature variation near the sea surface than is expected by the linear temperature profile assumed by F96, as suggested by *Zeng and Beljaars* [2005] and *Gentemann et al.* [2009].

[33] Figure 3 compares the variations of the amplitude of ΔSST with varying U and H_0, when H is given by $H = H_0[1 - \cos(2\pi t/T)]$. Dashed lines represent the bulk ΔSST from the old model, and thin and thick solid lines represent the bulk and skin ΔSST from the new model. In the new model, the difference between skin and bulk ΔSST appears at $U < 3 - 4$ m s^{-1}, and it can be as large as 4 K, when $U = 1$ m s^{-1} and $H_0 = 350$ W m^{-2}. The estimation from F96 is generally lower than from the new model, but it becomes equivalent at $U = 1$ m s^{-1}. Meanwhile, the skin ΔSST from the present model is still lower than the prediction from ZB05 at the range of larger U ($U > 3$ m s^{-1}), where ZB05 is known to overestimate ΔSST substantially; for example, ΔSST from ZB05 at $H = 350$ W m^{-2} and $U = 4$ m s^{-1} is about 1.8 K [*Bellenger and Duvel*, 2009, Figure 7].

4.2. Distribution of ΔSST Simulated From the Coupled Model

[34] Figure 4 shows the distribution of bulk and skin ΔSST on June 5th, 2008, simulated by the coupled model.

Table 1. RMSE, Bias, and Correlation Coefficient R of ΔSST Between Model Output and Other Sources

ΔSST	RMSE (K)	Bias (K)	R
model versus KK03 (bulk)	0.19	–0.10	0.84
model versus F96 (skin)	0.55	0.27	0.60
model versus buoy data (bulk)	0.45	0.07	0.31
model versus satellite data (skin)	0.72	0.18	0.05

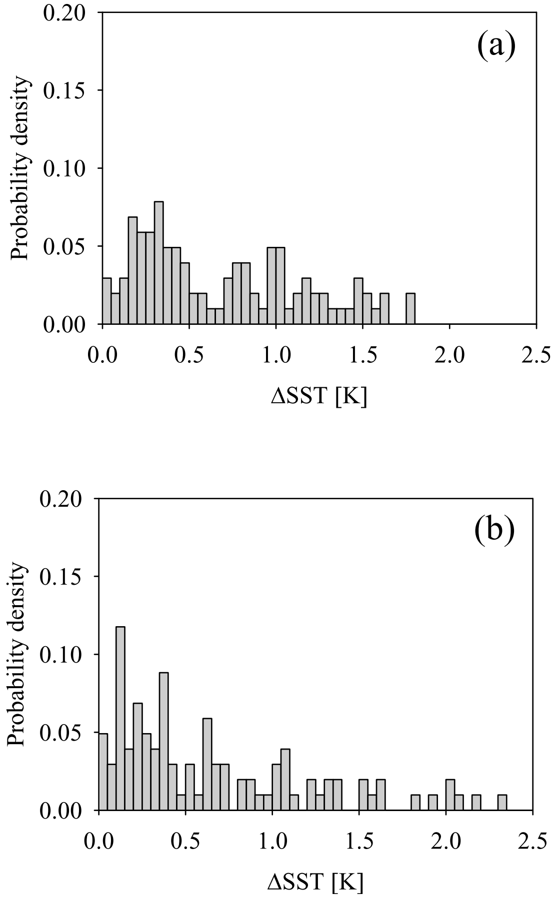

Figure 11. Probability density functions of ΔSST (model data are sampled only in the region where buoy data are available). (a) Bulk ΔSST from the model and (b) bulk ΔSST from buoy data.

Here ΔSST is defined by the difference of SST at 0900 LST and 1500 LST. The patterns of bulk and skin ΔSST are similar to each other, except that the skin ΔSST is higher than the bulk ΔSST, when ΔSST is very large (bulk ΔSST > 1 K). The corresponding daily peak solar radiation and daily mean wind fields are shown in Figure 5.

[35] The region with larger bulk and skin ΔSST generally corresponds to the region where the daily mean wind is smaller than 3 m s^{-1}, such as in the Pacific Ocean south of 25°N, the East China Sea, and the Sea of Okhotsk. The close correlation with the wind field reflects the fact that insolation is usually stronger in the region of weak wind. However, in some regions, as in the south of Korea, wind is strong in spite of strong insolation, and ΔSST remains low.

[36] Figures 6 and 7 show that the model reproduces well the observed daily mean sea level pressure (SLP) and cloud fraction at 1100 LST. Here the daily mean values are obtained over the same time period as the model. For observation data, the NCEP Final Analysis (FNL) data is used for SLP, and the satellite image from MODIS level 1 and 2 data is used for cloud fraction (http://ladsweb.nascom.nasa.gov/browse_images/l2_browser.html). It implies that the general feature of the atmospheric forcing is equivalent to the observed one. It should be also mentioned that the predictability is improved slightly by coupling to the mixed layer model, compared to the atmosphere only model, although the difference is rather insignificant in the present case (not shown).

[37] Another interesting aspect of diurnal variation of SST is the timing of the peak SST. The probability density function, which is obtained from the data over the whole period (June 4−14, 2008), reveals that the peak temperature appears most frequently at 1500 LST, but there exists a large variation (Figure 8). The daily maximum SST appears during 1400–1600 LST in only 55.2% cases. It is consistent with the suggestion by *Koizumi* [1956] data that the peak temperature occurs around 1500 LST in summer and it occurs around 1300 LST in winter, which is confirmed from other in situ measurements too [*Kawamura et al.*, 2008; *Gentemann and Minnett*, 2008].

4.3. Comparison of ΔSST From the Regression Model and Satellite Data

[38] *Kawai and Kawamura* [2003, hereinafter KK03] suggested a regression model to evaluate the 1-m-depth ΔSST, as

$$\Delta SST = a(MS + H_l + e)^2 + b[\ln(U)] + c(MS + H_l + e)^2[\ln(U)] + d \tag{15}$$

where MS, H_l, and U are the daily mean values of solar radiation, latent heat flux (upward is negative), and wind speed at z = 10 m, respectively, and a, b, c, d, and e are constants. They compared the ΔSST predicted from (15) with buoy data in the western Pacific, and concluded that, apart from a marginal sea, the model estimation has RMSE of 0.2–0.3 K, and bias less than 0.1 K. They also argued that buoy data are affected by artificial mixing induced by the buoy hull moving from the sea surface to this depth. It implies that ΔSST predicted by (15) may actually represent the ΔSST mixed over Δz = 1 m. We compare ΔSST from KK03 with the bulk ΔSST based on T_1 from the present model. Figure 9a shows the distribution of the bulk ΔSST calculated from (15), using the coupled model results for the atmospheric forcing. The distribution pattern and magnitude of ΔSST are similar to model results, shown in Figure 4a.

[39] The distribution of the skin ΔSST from F96, which is also obtained using the coupled model results for the atmospheric forcing, shows the similar pattern to Figure 4b, too. However, ΔSST tends to be smaller in most regions, except in the region with small U in the Pacific Ocean south of 25°N. The starting time of accumulation of heat and momentum fluxes was set to be 0600 LST, as found by *Gentemann et al.* [2009].

[40] Data are not available in the region covered with cloud in the distribution of the skin ΔSST obtained from satellite data (Figure 9c). Data with negative ΔSST are also eliminated, because the integrated surface heat flux during the period is always positive. Note that the daily mean SST obtained by some satellite measurements, including those used here, represents the bulk SST, because algorithms in these cases are tuned by using buoy-observed SST, but its diurnal variation represents the skin SST [*Stuart-Menteth and Robinson*, 2003; *Kawai and Kawamura*, 2005]. The distribution of ΔSST from satellite data shows that the pattern is consistent with the model result, although large area is covered with cloud.

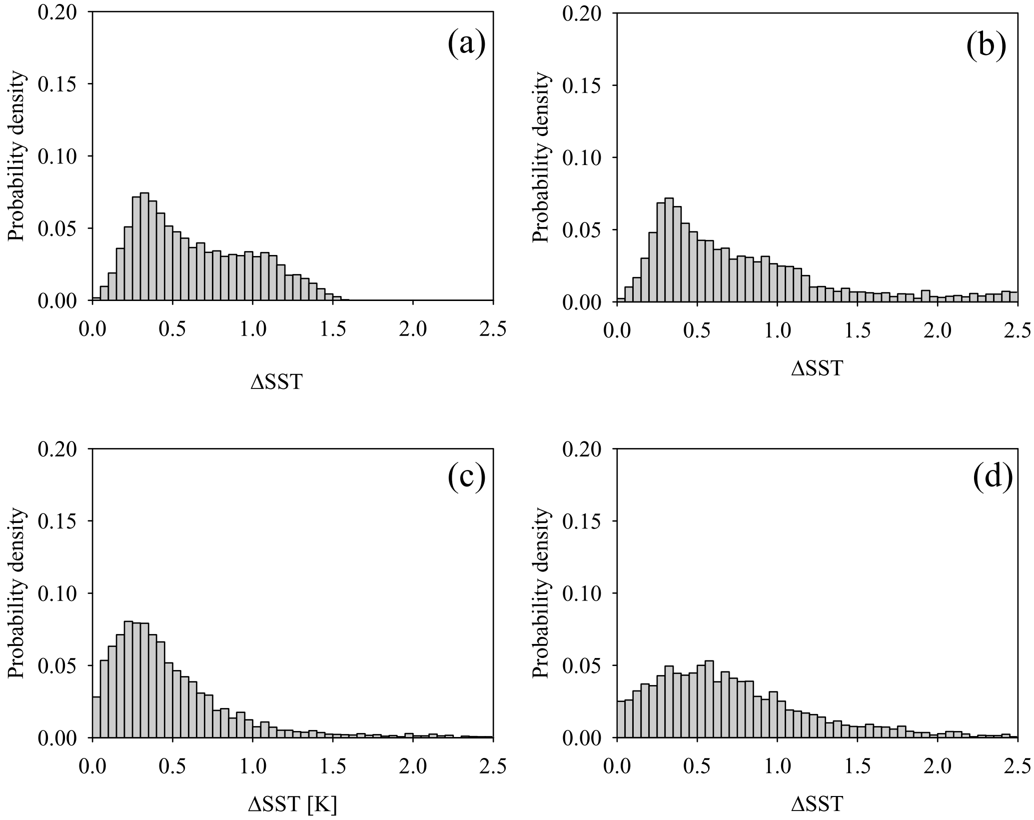

Figure 12. Probability density functions of ΔSST (model data are sampled only in the region where satellite data are available). (a) Bulk ΔSST from the model, (b) skin ΔSST from the model, (c) skin ΔSST from F96, and (d) skin ΔSST from satellite data.

[41] Figure 10 shows scatterplots which compare the bulk ΔSST from the coupled model with those from KK03 (Figure 10a) and buoy data (Figure 10c), and the skin ΔSST with those from F96 (Figure 10b) and satellite data (Figure 10d). For scatterplots the values of ΔSST averaged over 1° × 1° grid cells are used, and the whole 11 day data are used. Here, the bulk ΔSST from buoy data is obtained by the difference of the minimum SST during 7–10 LST and the maximum SST during 13–16 LST. Only 20–50 buoy data exist within these time spans per day.

[42] A good agreement is found between the bulk ΔSSTs from the coupled model and KK03. It suggests that the present mixed layer model can predict the bulk ΔSST reasonably, as long as the atmospheric forcing is accurate. On the other hand, the skin ΔSST obtained from F96 tends to be smaller than from the coupled model, as expected from Figures 2 and 3. Large scatter at larger ΔSST in Figure 10b may be due to the fact that the skin ΔSST is sensitive to the temporal variation of heat and momentum fluxes in the coupled model, but it is not found by F96, which is based on the accumulated heat and momentum fluxes.

[43] The correlations of the model ΔSSTs with real observation data, such as buoy and satellite data, are low, because the surface forcing from the model does not match exactly with the one in the real ocean in spite of the resemblance in the large-scale weather pattern (Figures 6 and 7). Moreover, the high level of background noise in satellite data further deteriorates the correlation between two ΔSST data. The RMSE, bias, and correlation coefficient corresponding to Figure 10, are listed in Table 1. Similar scatterplots comparing ΔSST from model results and satellite or buoy data were obtained previously by *Kawai and Kawamura* [2002], *Bellenger and Duvel* [2009], and *Tanahashi et al.* [2003]. Although the atmospheric forcing for model was estimated based on satellite data in these cases, instead of using the atmosphere-ocean mixed layer coupled model, the correlations between ΔSST data were still low, similar to Figures 10c and 10d.

[44] Considering the difficulty of matching these two data, we compare the probability density function of ΔSST. Even if the data do not match at identical locations, the similar probability density function of ΔSST is expected from the model, if the simulated weather pattern and the mixed layer model are realistic.

[45] Figure 11 compares the probability density function of the bulk ΔSST from the model and buoy data. The general pattern of distribution is similar, although the buoy data show larger variance. Note that the buoy data for ΔSST is sampled from the available data within the period of 3 h around 0900 LST and 1500 LST.

[46] Figure 12 compares the probability density function of skin ΔSSTs from the model, F96, and satellite data, together with the bulk ΔSST from the model. Similar distribution patterns are found in the skin ΔSSTs from the coupled model and satellite data, except for the large scatter of satellite data for small ΔSST (ΔSST < 0.5 K), whereas no data larger than 1.5 K appears in the bulk ΔSST from the model. The tendency of underestimation of ΔSST is

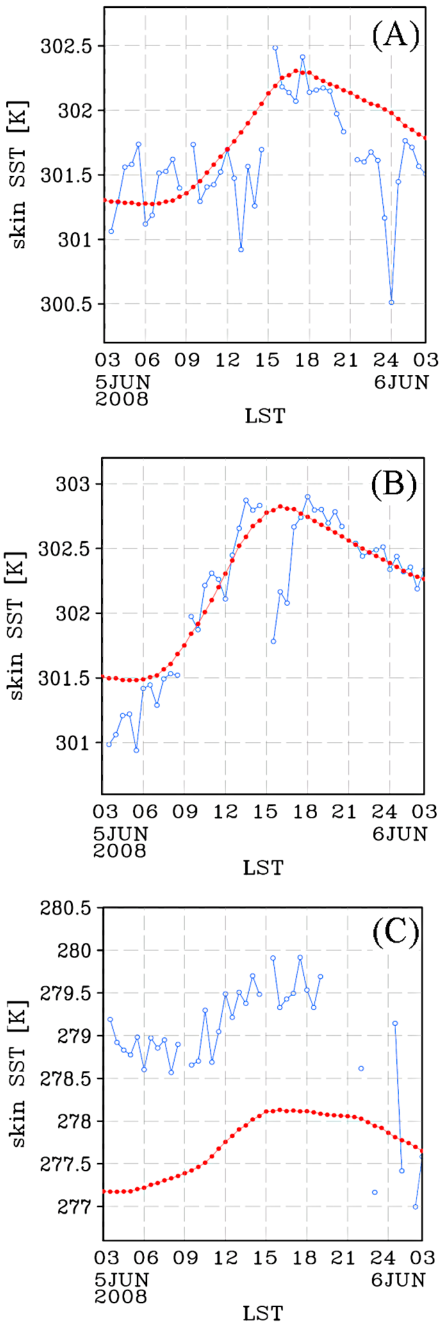

Figure 13. Time series of SST from model output (red) and satellite data (blue): (a) 20°N, 130°E, (b) 25°N, 146°E, and (c) 46°N, 145°E (locations of Figures 13a–13c are found in Figure 9c).

observed by F96. The evaluation of the percentage of the skin ΔSST larger than 1.5 K gives 9.6%, 7.1% and 2.8%, respectively for the coupled model, satellite data, and F96. Note that the underestimation of ΔSST by F96 is reported in the previous work [*Gentemann et al.*, 2009]. Furthermore, it is worth mentioning that the ΔSSTs from satellites themselves can be underestimated because of the problem in the algorithm of converting the measured infrared radiances into SST [*Merchant et al.*, 2009a, 2009b].

[47] The time series of skin SST at several locations show that the present model is able to predict well not only ΔSST, but also the continuous diurnal variation of SST (Figure 13). Even at the location where there exists a large difference in the initial SSTs between the satellite data and the FNL data used in the present model, they follow the similar pattern of diurnal variation (Figure 13c).

[48] Finally, when the time series of ΔSST averaged over the grid size 5° × 5° are plotted for the regions, where satellite data are available mostly during the period (135–140°W, 16–21°N and 142.5–147.5°E, 20–25°N), a good agreement is found between model output and satellite data (Figure 14).

4.4. Distributions of Subsurface Temperature

[49] One of the advantages of the mixed layer model, in contrast to satellite data, is to provide information below the sea surface. The information on temperature profile below the sea surface is important not only for many oceanographical applications, but also for the assimilation of satellite SST data into the ocean model, because the surface boundary condition of temperature in the ocean model implies the mean temperature of the first grid, rather than the skin SST measured by a satellite.

[50] The distributions of diurnal warming at $z = 5$ m, ΔT_5, reveals that the ΔSST larger than 1 K, as shown in Figure 4, never reaches to this depth in the present model (Figure 15a). On the contrary, ΔT_5 is smaller in this region, because heat cannot be transported to this depth (Figure 2b), as in the

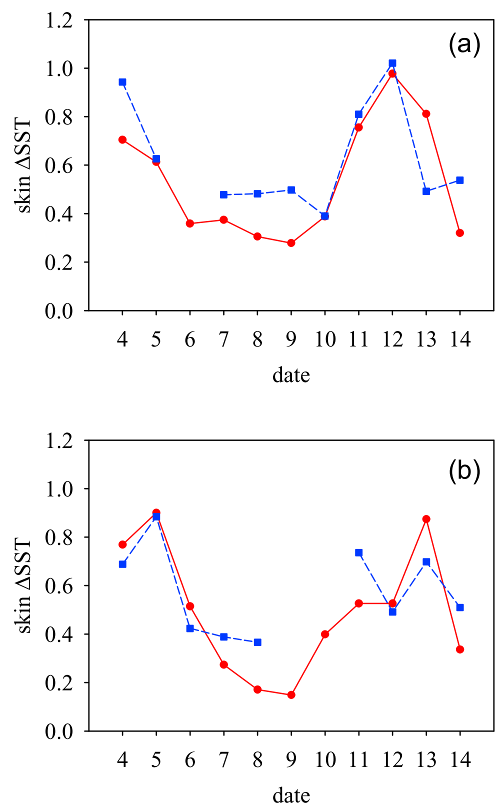

Figure 14. Variations of ΔSST during the period June 4–14, 2008 from model output (red) and satellite data (blue): (a) 135–140°E, 16–21°N and (b) 142.5–147.5°E, 20–25°N. Locations of Figures 14a and 14b are found in Figure 9c.

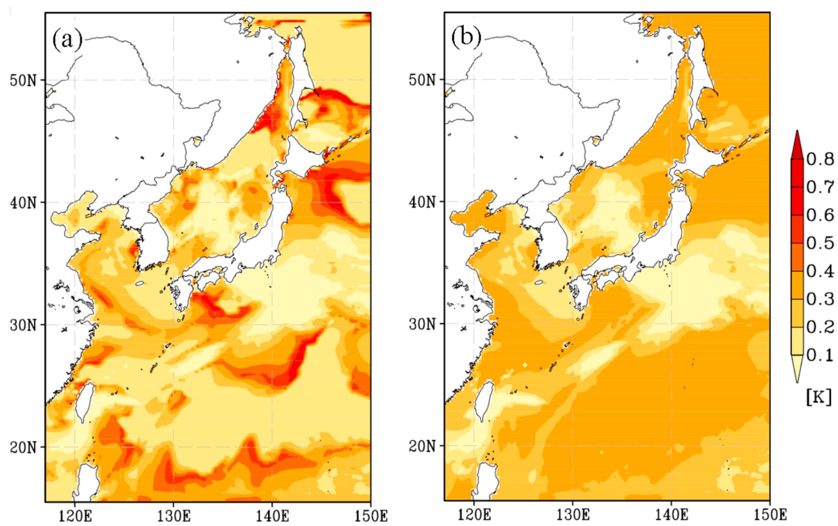

Figure 15. Distributions of diurnal warming below the sea surface from the model (June 5, 2008): (a) z = 5 m and (b) averaged over z = 0–10 m.

Pacific Ocean south of 25°N. As expected, ΔT_5 is also very small in the region of weak insolation, as in the southeast of Japan. Relatively larger values of ΔT_5 appears in the region where both solar radiation and wind speed are larger, as in the East China Sea and the east of the Hokkaido Island. In this case turbulent mixing transports heat to a deeper depth.

[51] On the other hand, Figure 15b reveals that the distribution of diurnal warming averaged over the top 10 m, $\Delta\overline{T}$, is more closely related with that of peak solar radiation (*PS*), than of the daily mean wind speed (*U*) (Figures 4 and 5), and never higher than 0.5 K. The evaluation of correlation coefficients with *PS* and *U* from Figures 4, 5, and 15 gives 0.23 and 0.39 for ΔSST, but 0.51 and 0.37 for $\Delta\overline{T}$. It is in contrast to the fact that the distribution of ΔSST is more closely related with that of wind speed.

[52] Figure 15b also implies that one should be careful when assimilating satellite data into the ocean model. The appropriate SST, which must be used as the surface boundary condition in the ocean model with the grid thickness 10 m, should be the one represented by Figure 15b, rather than the skin SST, measured by a satellite. The difference between the skin ΔSST and $\Delta\overline{T}$ can be as large as 3°C (Figures 4b and 15b).

5. Conclusion

[53] The present paper shows that the diurnal warming of SST can be successfully predicted using an atmosphere-ocean mixed layer coupled model. For this purpose, a new mixed layer model is developed, which is able to reproduce realistic temperature profiles under the various atmospheric conditions, ranging from the formation of a diurnal thermocline under strong wind to the appearance of strong near surface stratification under weak wind, as shown in Figure 2. Predictability of the model is verified by the comparison with satellite and buoy data, including scatterplots, time series and probability density functions of ΔSST. The predictability of the bulk ΔSST is confirmed by the agreement with the regression model by *Kawai and Kawamura* [2003]. On the other hand, the present model is shown to improve the problem of the model by *Fairall et al.* [1996] associated with the underestimation of the skin ΔSST. In addition, the diurnal variation of temperature profiles below the sea surface, whose information is not available from satellite data, is investigated based on model output.

[54] Once the atmosphere-ocean mixed layer coupled model is developed successfully, it is expected to contribute to various applications. First, the predicted SST data can contribute to the production of reliable SST database by complementing satellite data [e.g., *Donlon et al.*, 2007] with its capability of providing continuous information regardless of cloud condition. The information on the diurnal variation of SST will also help to merge satellite data measured at different times of the day. Second, the coupling of the ocean mixed layer model to the NWP model can improve the predictability by realizing more realistic air-sea interaction. Third, the information on temperature profiles below the sea surface will be useful for various oceanographic applications and for the assimilation of satellite SST data to the ocean model. Finally, the coupled model allows us to investigate air-sea interaction directly.

[55] Meanwhile, for the practical application of the coupled model, further improvement of the model and verification with more accurate observation data are necessary. Verification of the model by the comparison of temperature profiles from the ocean station, in which simultaneous atmospheric forcing data are available, will support the validity of the model further. In order to predict the whole diurnal cycle more accurate initial condition of the ocean must be provided, because convective deepening of the mixed layer and the consequent decrease of SST are affected by the temperature profile below the mixed layer, especially in winter. One may need to include the effects of advection and upwelling to apply to the condition of hurricane.

[56] **Acknowledgments.** This study was supported by the Korea Meteorological Administration Research and Development Program under grant CATER 2009–2258. Calculations were performed by using the supercomputing resources of the KISTI.

References

Bellenger, H., and J.-P. Duvel (2009), An analysis of tropical ocean diurnal warm layers, *J. Clim.*, *22*, 3629–3646, doi:10.1175/2008JCLI2598.1.

Bellenger, H., Y. Takayabu, T. Ushiyama, and K. Yoneyama (2010), Role of diurnal warm layers in the diurnal cycle of convection over the tropical Indian Ocean during MISMO, *Mon. Weather Rev.*, *138*, 2426–2433, doi:10.1175/2010MWR3249.1.

Bernie, D. J., S. J. Woolnough, J. M. Slingo, and E. Guilyardi (2005), Modeling diurnal and intraseasonal variability of the ocean mixed layer, *J. Clim.*, *18*, 1190–1202, doi:10.1175/JCLI3319.1.

Brainerd, K. E., and M. C. Gregg (1993), Diurnal restratification and turbulence in the oceanic surface mixed layer: 1. Observations, *J. Geophys. Res.*, *98*, 22,645–22,656, doi:10.1029/93JC02297.

Clayson, C. A., and A. Chen (2002), Sensitivity of a coupled single-column model in the tropics to treatment of the interfacial parameterizations, *J. Clim.*, *15*, 1805–1831, doi:10.1175/1520-0442(2002)015<1805:SOACSC>2.0.CO;2.

Clayson, C. A., and D. Weitlich (2007), Variability of tropical diurnal surface temperature, *J. Clim.*, *20*, 334–352, doi:10.1175/JCLI3999.1.

Cornillon, P., and L. Stramma (1985), The distribution of diurnal sea surface warming events in the western Sargasso Sea, *J. Geophys. Res.*, *90*, 11,811–11,815, doi:10.1029/JC090iC06p11811.

Craig, P. D., and M. L. Banner (1994), Modeling wave-enhanced turbulence in the ocean surface layer, *J. Phys. Oceanogr.*, *24*, 2546–2559, doi:10.1175/1520-0485(1994)024<2546:MWETIT>2.0.CO;2.

Dai, A., and K. E. Trenberth (2004), The diurnal cycle and its depiction in the Community Climate System Model, *J. Clim.*, *17*, 930–951, doi:10.1175/1520-0442(2004)017<0930:TDCAID>2.0.CO;2.

Davis, C., et al. (2008), Prediction of landfalling hurricanes with the advanced hurricane WRF model, *Mon. Weather Rev.*, *136*, 1990–2005, doi:10.1175/2007MWR2085.1.

Delnore, V. E. (1972), Diurnal variations of temperature and energy budget for the ocean mixed layer, *J. Phys. Oceanogr.*, *2*, 239–247, doi:10.1175/1520-0485(1972)002<0239:DVOTAE>2.0.CO;2.

Donlon, C. J., P. J. Minnett, C. Gentemann, T. J. Nightingale, I. J. Barton, B. Ward, and M. J. Murray (2002), Toward improved validation of satellite sea surface skin temperature measurements for climate research, *J. Clim.*, *15*, 353–369, doi:10.1175/1520-0442(2002)015<0353:TIVOSS>2.0.CO;2.

Donlon, C. J., et al. (2007), The Global Ocean Data Assimilation Experiment High-Resolution Sea Surface Temperature Pilot Project, *Bull. Am. Meteorol. Soc.*, *88*, 1197–1213, doi:10.1175/BAMS-88-8-1197.

Duan, A., C. Sui, and G. Wu (2008), Simulation of local air-sea interaction in the great warm pool and its influence on Asian monsoon, *J. Geophys. Res.*, *113*, D22105, doi:10.1029/2008JD010520.

Dudhia, J. (1989), Numerical study of convection observed during the winter monsoon experiment using a mesoscale two-dimensional model, *J. Atmos. Sci.*, *46*, 3077–3107, doi:10.1175/1520-0469(1989)046<3077:NSOCOD>2.0.CO;2.

Dybbroe, A., K.-G. Karllson, and A. Thoss (2005), NWCSAF AVHRR cloud detection and analysis using dynamic thresholds and radiative transfer modeling. Part I: Algorithm description, *J. Appl. Meteorol.*, *44*, 39–54, doi:10.1175/JAM-2188.1.

Fairall, C. W., E. F. Bradley, J. C. Godfrey, G. A. Wick, J. B. Edson, and G. S. Young (1996), Cool-skin and warm-layer effects on sea surface temperature, *J. Geophys. Res.*, *101*, 1295–1308, doi:10.1029/95JC03190.

Flament, C. W., J. Firing, M. Sawyer, and C. Trefois (1994), Amplitude and horizontal structure of a large diurnal sea surface warming event during the coastal ocean dynamics experiment, *J. Phys. Oceanogr.*, *24*, 124–139.

Gentemann, C. L., and P. J. Minnett (2008), Radiometric measurements of ocean surface thermal variability, *J. Geophys. Res.*, *113*, C08017, doi:10.1029/2007JC004540.

Gentemann, C. L., C. J. Donlon, A. Stuart-Menteth, and F. J. Wentz (2003), Diurnal signals in satellite sea surface temperature measurements, *Geophys. Res. Lett.*, *30*(3), 1140, doi:10.1029/2002GL016291.

Gentemann, C. L., P. J. Minnett, P. Le Borge, and C. J. Merchant (2008), Multi-satellite measurements of large diurnal warming events, *Geophys. Res. Lett.*, *35*, L22602, doi:10.1029/2008GL035730.

Gentemann, C. L., P. J. Minnet, and B. Ward (2009), Profiles of ocean surface heating (POSH): A new model of upper ocean diurnal warming, *J. Geophys. Res.*, *114*, C07017, doi:10.1029/2008JC004825.

Haarsma, R. J., E. J. D. Campos, W. Hazeleger, C. Severijns, A. Piola, and F. Molteni (2005), Dominant modes of variability in the South Atlantic: A study with a hierarchy of ocean-atmosphere models, *J. Clim.*, *18*, 1719–1735, doi:10.1175/JCLI3370.1.

Hasumi, H., and S. Emori (2004), K-1 coupled GCM (MIROC) description, *Tech. Rep. 1*, 34 pp., Univ. of Tokyo, Tokyo.

Hong, S. Y., J. Dudhia, and S.-H. Chen (2004), A revised approach to ice microphysical processes for the bulk parameterization of clouds and precipitation, *Mon. Weather Rev.*, *132*, 103–120, doi:10.1175/1520-0493(2004)132<0103:ARATIM>2.0.CO;2.

Kain, J. S. (2004), The Kain-Fritsch convective parameterization: An update, *J. Appl. Meteorol.*, *43*, 170–181, doi:10.1175/1520-0450(2004)043<0170:TKCPAU>2.0.CO;2.

Kalnay, E., et al. (1996), The NCEP/NCAR 40-Year Reanalysis Project, *Bull. Am. Meteorol. Soc.*, *77*, 437–471, doi:10.1175/1520-0477(1996)077<0437:TNYRP>2.0.CO;2.

Kawai, Y., and H. Kawamura (2000), Study on a platform effect in the in situ sea surface temperature observations under weak wind and clear sky conditions using numerical models, *J. Atmos. Oceanic Technol.*, *17*, 185–196, doi:10.1175/1520-0426(2000)017<0185:SOAPEI>2.0.CO;2.

Kawai, Y., and H. Kawamura (2002), Evaluation of the diurnal warming of sea surface temperature using satellite-derived marine meteorological data, *J. Oceanogr.*, *58*, 805–814, doi:10.1023/A:1022867028876.

Kawai, Y., and H. Kawamura (2003), Validation of daily amplitude of sea surface temperature evaluated with a parametric model using satellite data, *J. Oceanogr.*, *59*, 637–644, doi:10.1023/B:JOCE.0000009593.84009.d2.

Kawai, Y., and H. Kawamura (2005), Spatial and temporal variations of model-derived diurnal amplitude of sea surface temperature in the western Pacific Ocean, *J. Geophys. Res.*, *110*, C08012, doi:10.1029/2004JC002652.

Kawai, Y., and A. Wada (2007), Diurnal sea surface temperature variation and its impact on the atmosphere and ocean: A review, *J. Oceanogr.*, *63*, 721–744, doi:10.1007/s10872-007-0063-0.

Kawamura, H., H. Qin, and K. Ando (2008), In-situ diurnal sea surface temperature variations and near-surface thermal structure in the tropical hot event of the Indo-Pacific warm pool, *J. Oceanogr.*, *64*, 847–857, doi:10.1007/s10872-008-0070-9.

Koizumi, M. (1956), Researches on variations of oceanographic conditions in the region of the ocean weather station "Extra" in the north Pacific Ocean (IV): On the diurnal variation in air and sea-surface temperatures, *Pap. Meteorol. Geophys.*, *7*, 145–154.

Lebeaupin Brossier, C., and P. Drobinski (2009), Numerical high-resolution air-sea coupling over the Gulf of Lions during two tramontane/mistral events, *J. Geophys. Res.*, *114*, D10110, doi:10.1029/2008JD011601.

McClain, E. P., W. P. Pichel, and C. C. Walton (1985), Comparative performance of AVHRR-based multichannel sea surface temperature, *J. Geophys. Res.*, *90*, 11,587–11,601, doi:10.1029/JC090iC06p11587.

Mellor, G. L., and T. Yamada (1982), Development of a turbulence closure model for geophysical fluid problems, *Rev. Geophys.*, *20*, 851–875, doi:10.1029/RG020i004p00851.

Melville, W. K. (1996), The role of surface-wave breaking in air-sea interaction, *Annu. Rev. Fluid Mech.*, *28*, 279–321, doi:10.1146/annurev.fl.28.010196.001431.

Merchant, C. J., M. J. Filipiak, P. Le Borgne, H. Roquet, E. Autret, J.-F. Piollé, and S. Lavender (2008), Diurnal warm-layer events in the western Mediterranean and European shelf seas, *Geophys. Res. Lett.*, *35*, L04601, doi:10.1029/2007GL033071.

Merchant, C. J., A. R. Harris, H. Roquet, and P. Le Borgne (2009a), Retrieval characteristics of non-linear sea surface temperature from the Advanced Very High Resolution Radiometer, *Geophys. Res. Lett.*, *36*, L17604, doi:10.1029/2009GL039843.

Merchant, C. J., P. Le Borgne, H. Roquet, and A. Marsouin (2009b), Sea surface temperature from a geostationary satellite by optimal estimation, *Remote Sens. Environ.*, *113*, 445–457, doi:10.1016/j.rse.2008.10.012.

Mlawer, E. J., S. J. Taubnam, P. D. Brown, M. J. Iacono, and S. A. Clough (1997), Radiative transfer for inhomogeneous atmospheres: RRTM, a validated correlated-k model for the longwave, *J. Geophys. Res.*, *102*, 16,663–16,682, doi:10.1029/97JD00237.

National Institute of Meteorological Research (2009), Research for the meteorological observation technology and its application, *Annu. Rep. 2009*, 215 pp., Seoul.

Niiler, P. P., and E. B. Kraus (1977), One-dimensional models of the upper ocean, in *Modelling and Prediction of the Upper Layers of the Ocean*, edited by E. B. Kraus, pp. 143–172, Pergamon, New York.

Noh, Y. (1996), The dynamics of the formation of a diurnal thermocline in the oceanic mixed layer, *J. Phys. Oceanogr.*, *26*, 2183–2195, doi:10.1175/1520-0485(1996)026<2183:DODTFI>2.0.CO;2.

Noh, Y., and H. J. Kim (1999), Simulation of temperature and turbulence structure of the oceanic boundary layer with the improved near-surface process, *J. Geophys. Res.*, 15,621–15,634, doi:10.1029/1999JC900068.

Noh, Y., C. J. Jang, T. Yamagata, P. C. Chu, and C. H. Kim (2002), Simulation of more realistic upper ocean process from an OGCM with a new ocean mixed layer model, *J. Phys. Oceanogr.*, *32*, 1284–1307, doi:10.1175/1520-0485(2002)032<1284:SOMRUO>2.0.CO;2.

Noh, Y., W. G. Cheon, S.-Y. Hong, and S. Raasch (2003), Improvement of the K-profile model for the planetary boundary layer based on large eddy simulation data, *Boundary Layer Meteorol.*, *107*, 401–427, doi:10.1023/A:1022146015946.

Noh, Y., H. S. Min, and S. Raasch (2004), Large eddy simulation of the ocean mixed layer: The effects of wave breaking and Langmuir circulation, *J. Phys. Oceanogr.*, *34*, 720–735, doi:10.1175/1520-0485(2004)034<0720:LESOTO>2.0.CO;2.

Noh, Y., Y. J. Kang, T. Matsuura, and S. Iizuka (2005), Effect of the Prandtl number in the parameterization of vertical mixing in an OGCM of the tropical Pacific, *Geophys. Res. Lett.*, *32*, L23609, doi:10.1029/2005GL024540.

Noh, Y., G. Goh, S. Raasch, and M. Gryschka (2009), Formation of a diurnal thermocline in the ocean mixed layer simulated by LES, *J. Phys. Oceanogr.*, *39*, 1244–1257, doi:10.1175/2008JPO4032.1.

Noh, Y., G. Goh, and S. Raasch (2010), Examination of the mixed layer deepening process during convection using LES, *J. Phys. Oceanogr.*, *40*, 2189–2195, doi:10.1175/2010JPO4277.1.

Noh, Y., G. Goh, and S. Raasch (2011), Influence of Langmuir circulation on the deepening of the wind-mixed layer, *J. Phys. Oceanogr.*, *41*, 472–484, doi:10.1175/2010JPO4494.1.

Paulson, C. A., and J. J. Simpson (1981), The temperature difference across the cool skin of the ocean, *J. Geophys. Res.*, *86*, 11,044–11,054, doi:10.1029/JC086iC11p11044.

Pimentel, S., K. Haines, and N. K. Nichols (2008), Modeling the diurnal variability of sea surface temperatures, *J. Geophys. Res.*, *113*, C11004, doi:10.1029/2007JC004607.

Price, J. F., R. A. Weller, and R. Pinkel (1986), Diurnal cycling: Observations and models of the upper ocean response to diurnal heating, cooling, and wind mixing, *J. Geophys. Res.*, *91*, 8411–8427, doi:10.1029/JC091iC07p08411.

Price, J. F., T. Sanford, and G. Z. Forristall (1994), Forced stage response to a moving hurricane, *J. Phys. Oceanogr.*, *24*, 233–260, doi:10.1175/1520-0485(1994)024<0233:FSRTAM>2.0.CO;2.

Rascle, N., and F. Ardhuin (2009), Drift and mixing under the ocean surface revisited: Stratified conditions and model-data comparisons, *J. Geophys. Res.*, *114*, C02016, doi:10.1029/2007JC004466.

Shinoda, T. (2005), Impact of the diurnal cycle of solar radiation on intraseasonal SST variability in the western equatorial Pacific, *J. Clim.*, *18*, 2628–2636, doi:10.1175/JCLI3432.1.

Skamarock, W. C., J. B. Klemp, J. Dudhua, D. O. Gill, D. M. Barker, M. G. Duda, X.-Y. Huang, W. Wang, and J. G. Powers (2008), A description of the Advanced Research WRF Version 3, *Tech. Note NCAR/TN-475+STR*, 125 pp., Natl. Cent. for Atmos. Res., Boulder, Colo.

Smith, S. D. (1988), Coefficients for sea surface wind stress, heat flux, and wind profiles as a function of wind speed and temperature, *J. Geophys. Res.*, *93*, 15,467–15,472, doi:10.1029/JC093iC12p15467.

Soloviev, A., and R. B. Lukas (1997), Observations of large diurnal warming events in the near-surface layer of the western equatorial Pacific warm pool, *Deep Sea Res., Part I*, *44*(6), 1055–1076, doi:10.1016/S0967-0637(96)00124-0.

Soloviev, A. V., and R. Lukas (2006), *The Near-Surface Layer of the Ocean: Structure, Dynamics, and Applications*, 222 pp., Springer, Dordrecht, Netherlands.

Soloviev, A. V., and P. Schlüssel (1996), Evolution of cool skin and direct air-sea gas transfer coefficient during daytime, *Boundary Layer Meteorol.*, *77*, 45–68, doi:10.1007/BF00121858.

Stommel, H., K. Saunders, W. Simmons, and J. Cooper (1969), Observations of the diurnal thermocline, *Deep Sea Res. Oceanogr. Abstr.*, *16*, 269–284.

Stuart-Menteth, A. C., and I. S. Robinson (2003), A global study of diurnal warming using satellite-derived sea surface temperature, *J. Geophys. Res.*, *108*(C5), 3155, doi:10.1029/2002JC001534.

Takaya, Y., J.-R. Bildot, A. C. M. Beljaars, and P. A. E. M. Janssen (2010), Refinements to a prognostic scheme of skin sea surface temperature, *J. Geophys. Res.*, *115*, C06009, doi:10.1029/2009JC005985.

Tanahashi, S., H. Kawamura, T. Takahashi, and H. Yusa (2003), Diurnal variations of sea surface temperature over the wide-ranging ocean using VISSR on board GMS, *J. Geophys. Res.*, *108*(C7), 3216, doi:10.1029/2002JC001313.

Ward, B., and M. A. Donelan (2006), Thermometric measurements of the molecular sublayer at the air-water interface, *Geophys. Res. Lett.*, *33*, L07605, doi:10.1029/2005GL024769.

Webster, P. J., C. A. Clayson, and J. A. Curry (1996), Clouds, radiation, and the diurnal cycle of sea surface temperature in the tropical western Pacific, *J. Clim.*, *9*, 1712–1730, doi:10.1175/1520-0442(1996)009<1712:CRATDC>2.0.CO;2.

Woolnough, S. J., F. Vitart, and M. A. Balmaseda (2007), The role of the ocean in the Madden-Julian Oscillation: Implications for MJO prediction, *Q. J. R. Meteorol. Soc.*, *133*, 117–128, doi:10.1002/qj.4.

Zeng, X., and A. Beljaars (2005), A prognostic scheme of sea surface skin temperature for modeling and data assimilation, *Geophys. Res. Lett.*, *32*, L14605, doi:10.1029/2005GL023030.

S.-Y. Hong, D.-H. Kim, E. Lee, and Y. Noh, Department of Atmospheric Sciences, Yonsei University, 134 Shinchon-dong, Seodaemun-gu, Seoul 120-749, South Korea. (noh@yonsei.ac.kr)

M.-J. Kim and M.-L. Ou, National Institute of Meteorological Research, 45 Gisangcheong-gil, Dongjak-gu, Seoul 156-720, South Korea.